Crustal deformation in northwestern Arabia from GPS measurements in Syria: Slow slip rate along the northern Dead Sea Fault

Abdulmutaleb Alchalbi,[1] Mohamad Daoud,[1] Francisco Gomez,[2] Simon McClusky,[3] Robert Reilinger,[3] Mohamad Abu Romeyeh,[1] Adham Alsouod,[1] Rayan Yassminh,[1] Basel Ballani,[1] Ryad Darawcheh,[4] Reda Sbeinati,[4] Youssef Radwan,[4] Riad Al Masri,[5] Mazhar Bayerly,[6] Riad Al Ghazzi[7] and Muawia Barazangi[8]

[1]*Syrian National Earthquake Center, Damascus, Syria*

[2]*Department of Geological Sciences, University of Missouri, Columbia, MO 65211, USA. E-mail: fgomez@missouri.edu*

[3]*Department of Earth, Atmospheric, and Planetary Sciences, Massachusetts Institute of Technology, Cambridge, MA 02142, USA*

[4]*Department of Geology, Syrian Atomic Energy Commission, Damascus, Syria*

[5]*Department of Civil Engineering, Damascus University, Damascus, Syria*

[6]*Department of Geology, Tishreen University, Latakia, Syria*

[7]*Syrian Virtual University, Damascus, Syria*

[8]*Institute for the Study of the Continents, Cornell University, Snee Hall, Ithaca, NY 14853, USA*

GJI Geodynamics and tectonics

SUMMARY

New Global Positioning System (GPS) measurements in NW Syria provide the first direct observations of near-field deformation associated with the northern Dead Sea fault system (DSFS) and demonstrate that the kinematics of the northern section of this transform plate boundary between the Arabian and Sinai plates deviate significantly from plate model predictions. Velocity estimates based on GPS survey campaigns in 2000, 2007 and 2008, demonstrate left-lateral shear along the northern DSFS with 1σ uncertainties less than 0.7 mm yr^{-1}. These velocities are consistent with an elastic dislocation model with a slip rate of 1.8–3.3 mm yr^{-1} and a locking depth of 5–16 km. This geodetically determined slip rate is about half of that reported farther south along the central section (Lebanese restraining bend) and the southern section (Jordan Valley and Wadi Araba) of the transform and consequently requires some deformation to occur away from the transform along other geological structures. The factor of two difference in slip rates along the transform is also consistent with differing estimates of total fault slip that have occurred since the mid Miocene: 20–25 km along the northern DSFS (in NW Syria) versus about 45 km along the southern DSFS segment. Some of the strain deficit may be accommodated by north–south shortening within the southwestern segment of the Palmyride fold belt of central Syria. Additionally, a distinct change in velocity occurs within the Sinai plate itself. These new GPS measurements, when viewed alongside the palaeoseismic record and the modest level of present-day seismicity, suggest that the reported estimates of recurrence time of large earthquakes ($M > 7$) along the northern section of the DSFS may be underestimated owing to temporal clustering of such large historical earthquakes. Hence, a revised estimate of the earthquake hazard may be needed for NW Syria.

Key words: Space geodetic surveys; Continental tectonics: strike-slip and transform; Neotectonics; Kinematics of crustal and mantle deformation; Asia.

1 INTRODUCTION

The Dead Sea fault system (DSFS) is the left-lateral transform boundary between the Arabian and Sinai plates as they converge with Eurasia. Despite a 2000+ year historical record of large and damaging earthquakes, the kinematics of the northern part of this transform have not been well documented. Although a palaeoseis-

mic estimate of the slip rate has recently been reported (Meghraoui *et al.* 2003), measurements of short-term (i.e. 'geodetic') deformation and strain accumulation have not been available. Comparisons of slip rates estimated at various timescales are essential to characterize time-variable tectonic activity, including earthquake clustering and time-dependent slip rates. In addition to the slip along the northern Dead Sea fault, there have also been

suggestions of active internal deformation within the northern Arabian Plate, most significantly along the Palmyride fold belt (Chaimov *et al.* 1990).

This study presents new GPS measurements from Syria that constrain crustal deformation in the northwestern part of the Arabian Plate and the northern part of DSFS (Fig. 1). The results provide a more complete picture of the active tectonic framework in this region and show unanticipated variations in the kinematics along the transform. In particular, the northern Dead Sea fault demonstrates slower GPS velocities (and a slower slip rate) than are observed along the sections of the transform farther south. Furthermore, the GPS velocities suggest possible ongoing shortening across the Palmyride fold belt. Overall, these results suggest that the kinematics of the northern DSFS deviate significantly from what is expected based on regional plate models that assume coherent Sinai and Arabia plates. Accordingly, the results presented here will have significant implications for revising plate models, as well as the regional earthquake hazard.

2 TECTONIC SETTING

The northwestern region of the Arabian Plate encompasses several active tectonic elements including the DSFS, the Arabian-Eurasian continental collision in southern Turkey (Bitlis-Zagros fold-thrust belt), the intracontinental Palmyride fold-thrust belt, and the Euphrates depression (Fig. 1). The left-lateral DSFS bounds northwestern Arabia for nearly 800 km, from the Gulf of Aqaba northward to the East Anatolian fault, and is generally subdivided into three sections: (1) A southern section from the Gulf of Aqaba (Red Sea) through the Jordan Valley; (2) A central, NE–SW striking restraining bend through Lebanon and SW Syria and (3) A N–S striking section adjacent to the Syrian Coast Range (Brew *et al.* 2001). Additionally, the Kara Su Valley fault (southern Turkey) has been considered part of the northern DSFS (e.g. Westaway 2004). A total of 105 km of slip since the Cretaceous is documented along the southern DSFS (Freund *et al.* 1970; Hatcher *et al.* 1981; Quennell 1984), and about 45 km since the Early Pliocene when the DSFS
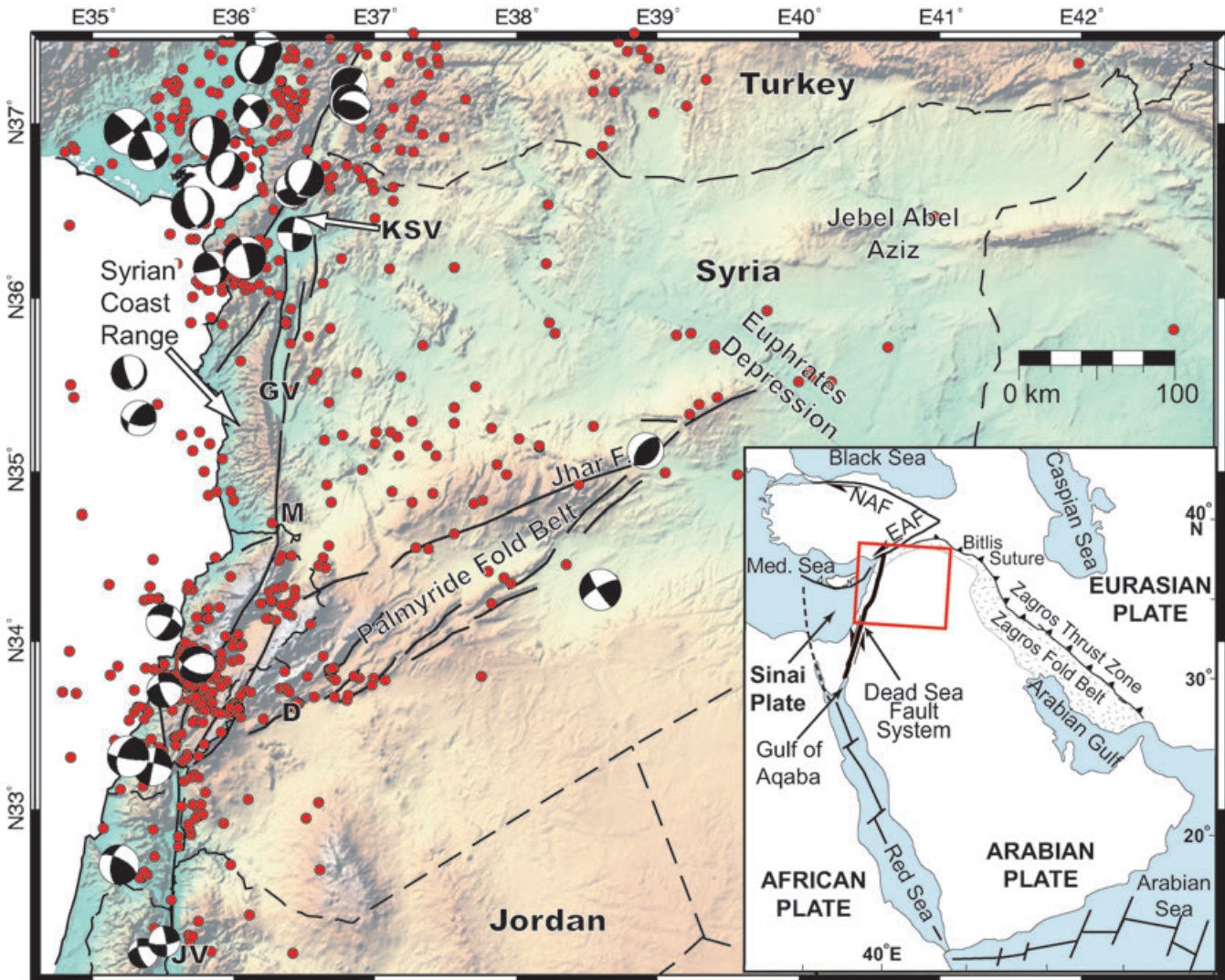

Figure 1. Seismicity and major neotectonic elements of Syria and the adjacent area. Heavy lines denote major faults. Red dots denote earthquake epicentres (*M* > 2.5) located by the Syrian National Earthquake Center (1994–2006). Focal mechanisms are from the compilation of Salamon *et al.* (2003). Abbreviations of geographic features cited in text: D, Damascus; M, Misyaf; JV, Jordan Valley; GV, Ghab Valley; KSV, Kara Su Valley. Inset: regional plate tectonic setting. EAF, East Anatolian fault; NAF, North Anatolian fault.

reactivated (Hempton 1987). Estimates of total slip along the northern DSFS are more disputed, ranging from ~25 km (Chaimov *et al.* 1990) to 70–80 km (Freund *et al.* 1970), and 20–25 km since the Early Pliocene (Hempton 1987). The shorter estimates of displacement on the northern DSFS are based on Neogene volcanic features, whereas the larger estimates are based on apparent displacement of the ophiolite in southern Turkey.

Published plate models describing motion between the Arabian and Sinai plates are based on geological criteria (Joffe & Garfunkel 1987) and, more recently, GPS measurements. We regard the GPS-based estimates of Reilinger *et al.* (2006) and Wdowinski *et al.* (2004) as particularly robust owing to their bases in the analysis of daily data from continuous GPS stations, which yield the most precise velocity estimates. Considering the uncertainties on the corresponding Euler poles, the plate models of Reilinger *et al.* (2006) and Wdowinski *et al.* (2004) are statistically compatible with one another.

In addition to the DSFS, central Syria comprises the intraplate, Palmyride fold belt (Chaimov *et al.* 1990). Crustal shortening across the ~120-km-wide Palmyride fold belt has been minor, about 20–25 per cent, and has taken place intermittently since Late Cretaceous time (Chaimov *et al.* 1990)—about 40 Myr, prior to the initiation of the main phase of left slip along the DSFS. However, historically documented earthquakes (Sbeinati *et al.* 2005), instrumental seismicity (Fig. 1), and geomorphology (e.g. Abou Romieh *et al.* 2009) suggest ongoing activity in the Palmyride region. In addition to the Palmyride fold belt, other late Cenozoic deformation in northern Arabia has occurred in the Euphrates depression (Litak *et al.* 1997) and the Jebel Abdel Aziz (Brew *et al.* 1999).

Historical records of seismicity attest to the tectonic activity of the region (e.g. Ambraseys & Barazangi 1989; Ambraseys & Jackson 1998; Sbeinati *et al.* 2005). For example, the catalogue of Sbeinati *et al.* (2005) represents a comprehensive databank on the historical earthquakes for Syria and surroundings, covering more than 2000 yr. While it is certain that many small earthquakes are missing from the record, the historical catalogue of large, earthquakes ($M > 7$) seems relatively complete for the past 2000 yr. The occurrence of large earthquakes in the historical records contrasts with the relative lack of instrumentally recorded seismicity (e.g. Ambraseys & Jackson 1998); hence, the instrumental seismicity represents an apparent quiescence that may not accurately reflect the earthquake potential of the northern DSFS.

Near-field geodetic analyses of present-day deformation along the central and southern DSFS suggest slip rates of 4–6 mm yr^{-1} (Wdowinski *et al.* 2004; Mahmoud *et al.* 2005; Gomez *et al.* 2007; Le Beon *et al.* 2008), and these generally agree with regional plate models (e.g. Joffe & Garfunkel 1987; Wdowinski *et al.* 2004; Reilinger *et al.* 2006). These fault slip rates are also consistent with 1000–1300 yr mean return periods for strike-slip earthquakes within the Lebanese restraining bend (Gomez *et al.* 2003; Daeron *et al.* 2007; Nemer *et al.* 2008) and along the southern DSFS (Klinger *et al.* 2000; Ferry *et al.* 2007).

Pertinent to this study, the only Holocene estimate of slip rate along the northern DSFS is reported near the village of Misyaf (Fig. 1), where the DSFS left-laterally offsets a Roman aqueduct (older than AD 70 and younger than AD 30) by 13.6 ± 0.2 m suggesting a slip rate of 6.9 ± 0.1 mm yr^{-1} (Meghraoui *et al.* 2003). This has led to the suggestion of an earthquake gap along the northern DSFS (Meghraoui *et al.* 2003). However, as shown by Meghraoui *et al.* (2003), this total displacement resulted from a cluster of earthquakes that occurred between 100 AD and 1170 AD. Hence, this estimate may reflect a bias, as it does not clearly span a complete

'earthquake cycle' for the northern DSFS, if this section of the fault is characterized by temporal clustering of earthquakes along the same fault segment. Palaeoseismic analyses along the northern DSFS north of the Ghab Valley (Akyuz *et al.* 2006) also document the repetition of three faulting events along that segment occurring over ~1000 yr (859–1872 AD); the trench stratigraphy in that study spans too short of a time to ascertain whether this earthquake recurrence is quasi-periodic or clusters in time. Additionally, evidence of temporal earthquake clustering along the southern DSFS has been reported by Marco *et al.* (1996). Essential to testing the possibility of an earthquake gap is an independent estimate of the slip rate along the northern DSFS. To that end, and to constrain active deformation of the northern Arabian Plate, we here report and analyse near-field Global Positioning System (GPS) velocity estimates for the northern DSFS and across the Palmyride Mountains in Syria, and use these velocities to estimate the fault slip rate using elastic dislocation models.

3 GPS MEASUREMENTS AND DATA PROCESSING

The regional GPS network used in this study consists of 36 survey monuments (surveyed three times; see Table 1) and one continuous GPS station (UDMC in Damascus; Fig. 2). Monumentation at the 36 survey sites consist of 15 cm steel pins cemented into bedrock. The campaign sites were installed and initially measured in late 2000 and early 2001. During the initial survey campaign, each site was observed for at least 48 hr using Trimble 4000 SSE and SSI receivers with Trimble L1/L2 with ground plane geodetic antennae. The sites were remeasured in the summer of 2007 and, again, in the summer of 2008 by the Syrian National Earthquake Center for at least 24 hr each, using Thales DSNP 6502MK receivers and Leica AT504 Choke ring Antennae. In all surveys, data were logged with a 30 s sampling rate.

GPS data were processed following a standard, two-step procedure using the GAMIT/GLOBK software (Herring *et al.* 1997; Dong *et al.* 1998; King & Bock 1998). In the first step, loosely constrained estimates of station coordinates, orbital and Earth orientation parameters, and atmospheric zenith delays were determined from raw GPS observables using GAMIT. Robust models for antenna phase centres were used to account for differences in field equipment between the surveys; uncertainties in those phase models were propagated into the loosely constrained solutions. Data from the Syrian GPS network were analysed along with raw GPS data from other continuously operating GPS (CGPS) stations in the region. Data from survey campaigns were subdivided into 8–10 hr epochs (typically at 2400 UTC), so that multiple, loosely constrained solutions were available for each site during each given campaign. In addition to the times of the three survey campaigns in Syria, CGPS data, when available, were also analysed at numerous epochs between 2002 and 2005, corresponding with survey campaigns in Lebanon (Gomez *et al.* 2007). A summary of the CGPS stations and their observations epochs is provided in Table 1.

Subsequently, a global Kalman filter (GLOBK) was applied to the loosely constrained solutions and their associated covariances in order to estimate a self-consistent set of station coordinates and velocities. As part of this second step, a six-parameter Helmert transformation was estimated by minimizing the horizontal velocities of 37 globally distributed IGS stations with respect to the IGS00 realization of the ITRF 2000 no-net-rotation reference (NNR) frame. The WRMS of the residual velocities for the IGS stations into ITRF

4 A. Alchalbi et al.

Table 1. Summary of GPS observation campaigns used in this study.

Date[a]	2000/12	2002/04	2002/10	2003/09	2004/09	2005/09	2007/07	2008/07
Survey-Mode GPS								
Syria	X						X	X
Lebanon[b]		X	X	X	X	X		
Continuous GPS								
UDMC		X	X	X			X	X
LAUG			X	X	X	X	X	X
HUGS					X	X	X	X
								X
Other CGPS[c]								
BAHR	X	X	X	X	X	X	X	X
BSHM	X	X	X	X	X	X	X	X
CSAR					X	X	X	X
ELRO	X	X	X	X	X	X	X	X
GILB	X	X	X	X	X	X	X	X
HALY			X		X	X	X	
KABR	X	X	X	X	X	X	X	X
NAMA			X		X	X	X	
SOLA			X		X	X	X	
YIBL					X	X	X	X

[a]Dates expressed as year and month (YYYY/MM).
[b]Details on Lebanon survey campaigns are found in Gomez *et al.* (2007).
[c]Data provided from Scripps Orbital and Permanent Array (SOPAC) archive.

2000 was 0.8 mm yr^{-1}. During this process, obvious outliers in the continuous and campaign time series were identified and removed; data from individual survey campaigns were then amalgamated into a single epoch corresponding with each survey campaign. Data for sites in Lebanon spanning 2002–2005 (Gomez *et al.* 2007) were also included in the velocity stabilization (including regional CGPS sites, as stated above).

Accurate characterization of the uncertainties in the velocities is critical to avoid over interpretation of the small tectonic signal associated with the DSFS. It is well regarded that the formal, standard error of the GPS solution underestimates the true uncertainty in the GPS velocities (e.g. Zhang *et al.* 1997; McClusky *et al.* 2000). Detailed studies of CGPS data indicate that the noise in GPS time-series may be characterized by colored noise that varies from fractal white noise to fractal random walk (Zhang *et al.* 1997; Mao *et al.* 1999). However, by estimating relative velocities (i.e. defining 'local' plate reference frames), we implicitly remove the common mode component of the noise within the region and, thus, within the noise (McClusky *et al.* 2000). White noise error in GPS observations accounts for factors such as monument stability and setup errors. In GPS processing with GLOBK, white noise is added as a time-dependent, random walk error in the velocity estimation. In our study, we applied a random walk noise of 1.3 mm yr^{-2}, which represents the average of random walk noise estimated for CGPS sites in the eastern Mediterranean region by Reilinger *et al.* (2006). We believe this is justified owing to the use of extremely stable, fixed-height antenna masts during the 2007 and 2008 survey campaigns.

After stabilizing the reference frame, the site velocities were resolved to an Arabia-fixed reference frame, which facilitates assessing the local deformation. The reference frame was defined by minimizing the motion of six GPS sites distributed around Arabia (Fig. 2, inset); the WRMS of the residual velocities used to define the Arabian Plate is 1.0 mm yr^{-1}. Similarly, the velocities were also translated into a Eurasia-fixed reference frame that was defined using 26 CGPS sites within Eurasia (WRMS of residuals = 1.1 mm yr^{-1}). GPS velocities (in ITRF2000-NNR, Arabia-fixed and

Eurasia-fixed reference frames) for the sites around the northern DSFS are provided in Table 2. We estimate ITRF2000 euler pole for the Arabian Plate is 48.790 ± 0.9°N/5.133 ± 1.9°W/0.481 ± 0.019° Myr^{-1}. For comparison, the Eurasia–Arabia euler pole from this study, 26.843 ± 1.3°N/17.796 ± 1.5°W/0.385 ± 0.025° Myr^{-1}, is consistent with the pole reported by Reilinger *et al.* (2006). The error reported here is larger because Reilinger *et al.* analysed detailed time series for the regional CGPS sites, whereas our study only analysed data during the time periods of GPS survey campaigns in Syria and Lebanon.

4 RESULTS AND MODELLING

As shown in Fig. 2, the resulting velocity field depicts the general, left-lateral shear along the northern DSFS, although the magnitudes of the velocities crossing the northern segment in Syria appear to be smaller than for sites crossing the central DSFS. 1σ uncertainties for the survey sites in Syria are typically less than 0.7 mm yr^{-1} (Table 2). Additionally, GPS sites within the interior of Syria suggest possible contraction across the Palmyride fold belt. These are explored further below.

4.1 Slip rate and locking depth of the northern DSFS

In order to infer the slip rate for the northern DSFS, we examine profiles of the GPS velocities across the fault (see Fig. 2 for locations). The profile in NW Syria (Figs 3a and b) decomposes the velocities into motions parallel and perpendicular to the transform near Misyaf, located across the transform where it is a single fault trace. The velocities parallel to the transform (Fig. 3b) show a progressive increase in northward velocity from west to east— a pattern that is generally consistent with basic models of elastic strain accumulation (Savage & Burford 1973).

To infer possible slip rates, we apply a 1-D, elastic dislocation model across the northern DSFS. This standard analytical method follows the approach originally discussed by Savage & Burford (1973): This profile model assumes an infinitely long strike-slip
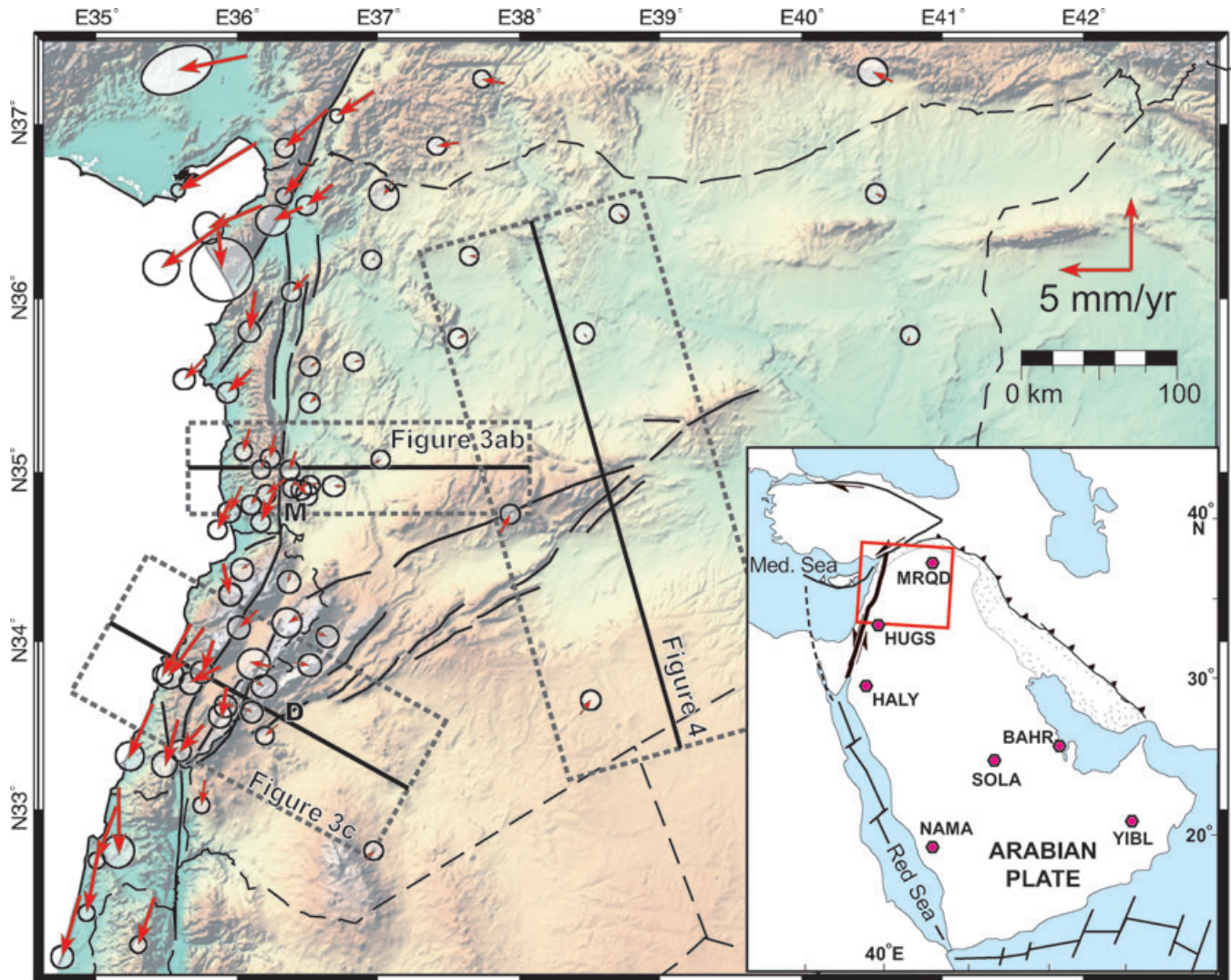
Figure 2. GPS velocities for the network used in this study (Arabia-fixed reference frame) with 1σ uncertainties. Abbreviations follow Fig. 1; GPS velocities in Turkey are from Reilinger *et al.* (2006); other velocities are from this study (see Table 2). Inset: map showing GPS sites used to estimate the Arabian Plate motion.

fault and expresses the station velocity, b, as a function of the long-term slip rate (V), fault locking depth (D) and distance from the fault (x)

$$b = (V/\pi)\tan{-1}(x/D). \tag{1}$$

Despite its simplicity, this model continues to provide basic, first-order kinematic parameters when applied to large, strike-slip faults globally (e.g. Lisowski *et al.* 1991; Pearson *et al.* 2000; Wright *et al.* 2001; Segall 2002; Wdowinski *et al.* 2004). The assumptions behind the 1-D profile are appropriate to the Misyaf section of the northern DSFS, as the transform consists of a single fault that traces from the northern end of the Lebanese Restraining Bend to the southern end of the Ghab Valley.

This analytical model permits assessing a range of values of fault slip rates and locking depths consistent with the GPS data using a grid search that explores the misfit of the model for a given range of parameters (locking depth and slip rate). Our implementation of the model also solves for a third parameter that applies a constant offset to the velocity in order to minimize the velocity at the fault (ideally zero). This grid search provided the basis for a 'Monte Carlo' simulation of the assumed, Gaussian noise level in the data

(Sandvol & Hearn 1994; Gomez *et al.* 2007). The 1σ contour for the profile is shown in Fig. 3(d). As demonstrated in Figs 3(a) and (d), the entire range of geological slip estimates (1.8–3.3 mm yr^{-1}) can be modeled to fit nearly all of the velocities, with locking depths of 5–16 km. As depicted in Fig. 3(d), the peak of the probability distribution corresponds with a slip rate of 2.5 mm yr^{-1} and a locking depth of 9 km. This locking depth is shallower than those reported from 1-D elastic dislocation profiles across the central and southern DSFS (e.g. Wdowinski *et al.* 2004; Gomez *et al.* 2007; Le Beon *et al.* 2008), and the profile across the central DSFS shown in Fig. 3(c) is provided for comparison. It should also be noted that the locking depths for dislocation models across the southern DSFS (Wdowinski *et al.* 2004; Le Beon *et al.* 2008), where the fault consists of a single segment, are also deeper than our result for the northern DSFS. As shown by the 1σ confidence ellipses in Fig. 3(d), the range of fault parameters that best fit the northern and central DSFS are statistically distinct.

The GPS-based slip rate along the northern DSFS is about half of the Holocene slip rate proposed by Meghraoui *et al.* (2003) based on the displaced Roman aqueduct near Misyaf. However, the palaeoseismically estimated slip rate in the study by Meghraoui

Table 2. Velocities of GPS sites shown in Fig. 2.

Site	Long	Lat	ITRF 2000		Arabia-fixed		Eurasia-fixed		σ E	σ N	corr
			Vel E	Vel N	Vel E	Vel N	Vel E	Vel N			
Syria											
AJSH	36.156	34.882	17.45	22.35	−0.55	−0.89	−5.17	10.82	0.45	0.45	−0.004
AKIL	37.634	35.800	16.99	23.63	−0.65	−0.29	−5.72	12.33	0.44	0.45	−0.006
ASAL	36.400	33.879	19.97	23.18	1.13	−0.18	−2.77	11.69	0.54	0.52	−0.04
BARN	36.404	34.948	17.91	22.85	−0.10	−0.51	−4.73	11.36	0.45	0.44	−0.002
BATH	36.091	35.247	17.24	21.69	−0.46	−1.52	−5.34	10.15	0.42	0.42	0.006
BLAN	36.754	34.914	17.46	23.55	−0.65	0.03	−5.23	12.11	0.52	0.47	−0.010
BMRA	36.343	34.957	16.67	22.29	−1.32	−1.04	−5.97	10.79	0.44	0.43	−0.003
BNAB	36.204	35.090	17.53	22.37	−0.32	−0.90	−5.08	10.85	0.43	0.43	0.003
DALY	36.270	35.215	17.44	21.68	−0.33	−1.62	−5.17	10.17	0.46	0.45	−0.004
DBSS	38.757	36.461	16.94	24.83	−0.46	0.41	−5.84	13.72	0.43	0.43	−0.001
DERS	36.419	35.118	17.44	22.08	−0.44	−1.28	−5.19	10.59	0.46	0.45	−0.006
DOHA	36.104	35.598	15.77	21.61	−1.66	−1.61	−6.78	10.07	0.50	0.47	0.012
HARM	36.508	36.146	15.9	22.19	−1.20	−1.21	−6.65	10.72	0.45	0.44	0.004
HASS	36.570	35.638	16.99	23.14	−0.52	−0.29	−5.61	11.68	0.47	0.45	−0.006
HBAB	36.033	34.915	17.08	21.41	−0.87	−1.78	−5.52	9.86	0.52	0.48	0.014
HMEH	40.596	36.584	17.13	25.54	−0.65	0.32	−5.85	14.73	0.45	0.45	−0.003
HMRY	36.503	34.965	17.55	22.56	−0.47	−0.84	−5.10	11.09	0.46	0.45	−0.018
HOOR	36.111	33.781	19.63	22.72	0.78	−0.51	−3.08	11.18	0.59	0.52	−0.006
HOWR	36.974	36.233	16.95	23.56	−0.19	−0.06	−5.64	12.16	0.46	0.45	0.001
JHAR	37.869	34.643	19.25	25.32	0.66	1.29	−3.59	14.06	0.46	0.45	−0.011
KATR	36.881	35.649	17.06	23.48	−0.51	−0.01	−5.58	12.06	0.46	0.44	−0.008
KBDD	38.437	33.571	20.24	25.27	0.70	0.99	−2.74	14.10	0.46	0.45	−0.010
KHAS	36.578	35.449	17.05	22.89	−0.61	−0.55	−5.57	11.43	0.47	0.46	−0.004
KHBZ	37.716	36.246	16.62	24.03	−0.69	0.08	−6.06	12.75	0.43	0.43	−0.011
KRIN	38.481	35.782	17.67	24.57	−0.19	0.27	−5.14	13.41	0.47	0.48	−0.018
MJDL	35.954	34.838	17.08	21.06	−0.91	−2.09	−5.52	9.50	0.44	0.43	−0.008
MRQD	40.761	35.754	18.57	25.76	0.12	0.47	−4.49	14.98	0.43	0.43	−0.006
MSHR	36.550	34.059	19.62	23.14	0.89	−0.29	−3.12	11.67	0.52	0.50	−0.028
MSHT	36.269	34.885	17.05	21.19	−0.97	−2.11	−5.59	9.68	0.45	0.44	−0.004
RAJO	36.681	36.664	14.92	22.01	−1.81	−1.47	−7.6	10.56	0.51	0.45	0.019
ROZA	36.010	33.625	18.07	23.14	−0.87	−0.04	−4.64	11.59	0.52	0.52	−0.011
RSHD	36.913	32.702	20.39	24.23	0.54	0.63	−2.49	12.82	0.44	0.43	−0.009
RSHM	35.769	35.659	15.91	21.63	−1.39	−1.43	−6.6	10.04	0.50	0.47	0.009
SALM	36.966	35.049	18.57	23.89	0.51	0.28	−4.13	12.49	0.43	0.42	0.000
SOBA	36.051	33.613	19.49	22.88	0.53	−0.32	−3.23	11.33	0.50	0.49	−0.012
TELF	36.573	34.934	17.51	23.29	−0.55	−0.15	−5.15	11.83	0.45	0.44	0.002
UDMC	36.285	33.510	18.31	22.61	−0.78	−0.70	−4.44	11.10	0.42	0.42	0.002
Lebanon											
ADAS	35.909	34.466	17.01	20.80	−1.25	−2.32	−5.62	9.23	0.75	0.71	0.011
ANJR	35.922	33.730	18.08	20.56	−0.75	−2.58	−4.61	8.99	0.74	0.76	−0.022
ARSL	36.467	34.164	17.39	22.37	−1.23	−1.02	−5.33	10.89	0.89	0.85	−0.011
BRKA	36.143	34.184	17.45	21.23	−1.08	−2.01	−5.23	9.70	0.76	0.74	−0.045
FRYA	35.829	34.005	17.23	20.08	−1.37	−3.02	−5.43	8.50	0.86	0.86	−0.008
HABT	36.084	34.451	17.24	20.90	−1.07	−2.31	−5.41	9.36	0.74	0.72	−0.007
HAYT	35.767	34.094	16.38	20.04	−2.15	−3.02	−6.27	8.45	0.75	0.75	0.016
HRML	36.379	34.412	17.79	22.21	−0.63	−1.13	−4.90	10.71	0.85	0.78	0.028
HZRT	35.880	33.869	17.41	21.43	−1.32	−1.69	−5.27	9.86	0.81	0.76	0.006
JIYE	35.411	33.651	17.18	19.19	−1.61	−3.70	−5.46	7.55	0.76	0.76	−0.022
JZIN	35.589	33.555	17.70	19.84	−1.21	−3.14	−4.97	8.22	0.76	0.75	−0.001
MCHK	35.771	33.526	17.05	20.80	−1.92	−2.26	−5.64	9.21	0.73	0.73	−0.051
RBDA	35.162	33.139	18.46	18.53	−0.66	−4.25	−4.19	6.85	0.81	0.79	0.025
TFEL	36.225	33.860	17.14	22.98	−1.68	−0.31	−5.58	11.46	0.90	0.92	−0.004
LAUG	35.674	34.115	17.17	19.86	−1.32	−3.16	−5.46	8.26	0.46	0.46	0.003
Other CGPS sites (data obtained from SOPAC archive)											
BAHR	50.608	26.209	28.09	28.26	0.66	−0.87	3.84	19.30	0.36	0.35	0.001
BSHM	35.023	32.779	18.50	18.25	−0.88	−4.47	−4.16	6.55	0.38	0.38	0.003
CSAR	34.89	32.488	18.67	18.42	−0.90	−4.23	−4.00	6.70	0.53	0.53	0.001
ELRO	35.771	33.182	18.95	21.32	−0.28	−1.75	−3.77	9.73	0.38	0.38	0.003
GILB	35.416	32.479	18.53	19.62	−1.17	−3.28	−4.2	7.98	0.38	0.38	0.003
HALY	36.100	29.139	23.37	21.87	1.01	−0.86	0.47	10.23	0.72	0.68	0.009

Table 2. (*Continued.*)

Site	Long	Lat	ITRF 2000		Arabia-fixed		Eurasia-fixed		σ E	σ N	corr
			Vel E	Vel N	Vel E	Vel N	Vel E	Vel N			
KABR	35.145	33.023	17.78	19.05	−1.44	−3.72	−4.88	7.37	0.38	0.38	0.003
NAMA	42.045	19.211	30.85	27.58	0.64	1.02	7.34	17.01	1.10	0.84	0.051
SOLA	46.401	24.911	28.25	26.73	0.89	−0.87	4.31	16.95	0.58	−.58	−0.001
YIBL	56.112	21.186	33.08	29.89	1.14	−1.01	8.64	22.06	0.51	0.49	−0.004
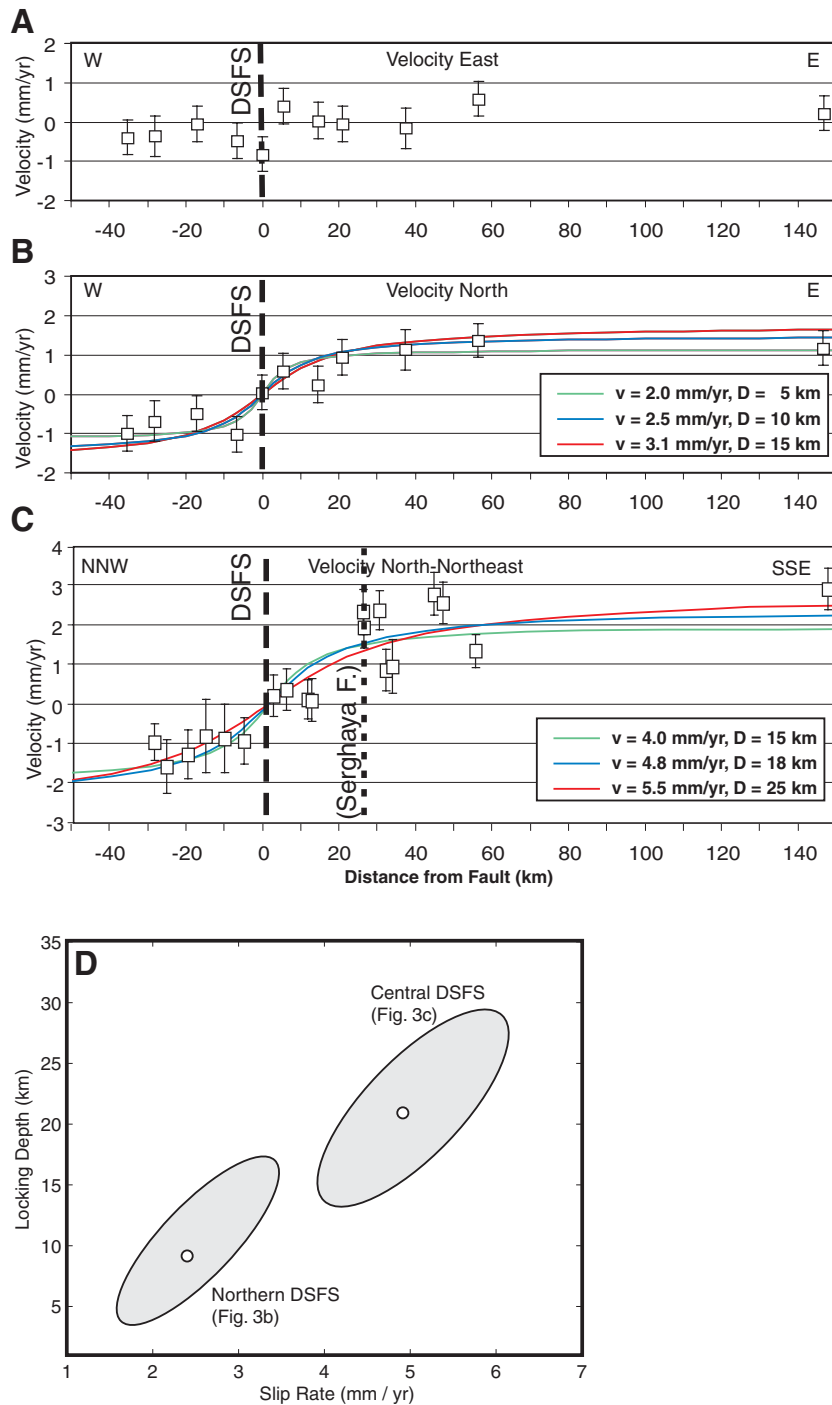
Figure 3. (a)–(b). Profile across the northern DSFS showing the GPS velocities perpendicular and parallel to the DSFS, respectively. (c) Profile depicting GPS velocities parallel to the Yammouneh fault (central DSFS) and corresponding elastic dislocation models (from Gomez *et al.* 2007). (d) A plot depicting the 1σ confidence limits on the slip rates and locking depths for profiles B and C based on a Monte Carlo simulation to estimate the noise level in the data. See Fig. 2 for locations of profiles. Heavy, dashed line shows where the DSFS crosses the profiles.

8   *A. Alchalbi* et al.

et al. (2003) is based on a ~3000 yr palaeoseismic record containing one earthquake cluster (three events during the first millennium: 115 AD, 700 AD–1030 AD and 1170 AD). Hence, without proper constraints on the repetition of the clusters, a large bias in the slip rate may be expected.

Although the kinematic modeling of GPS data reflects model-specific assumptions (e.g. the uniform elastic half-space used in this study), we believe the GPS analysis more accurately reflects the present-day slip rate for the northern DSFS. In general, elastic dislocation models have compared well with long-term slip rates along other major strike-slip faults in the region (e.g. Allen *et al.* 2004; Reilinger *et al.* 2006), as well as the central and southern DSFS (e.g. Mahmoud *et al.* 2005; Gomez *et al.* 2007; Le Beon *et al.* 2008). In any event, since the same basic model (1-D dislocation in a uniform elastic half-space) was applied to both the northern and the central DSFS, systematic errors owing to model-specific assumptions do not preclude the general result of a statistically distinct kinematic change along strike of the transform.

4.2 Internal deformation of Arabia

Aside from the motion of the DSFS, the new GPS results also permit a preliminary assessment of possible internal deformation within the northwestern Arabian Plate. Internal deformation of northern Arabia can be assessed from relative changes in GPS velocities.

Hence it is independent of the sites selected for the definition of the Arabian Plate motion. Although the distribution of GPS sites and the velocity uncertainties are insufficient to analyse individual structures within northern Arabia, the current network provides a basis to assess large, regional patterns of crustal deformation by identifying differences in coherent, block-like motions. Internal deformation, particularly associated with the Palmyride fold belt, has been suggested based on recent seismicity (e.g. Chaimov *et al.* 1990; Salamon *et al.* 1996), historically documented seismicity (Sbeinati *et al.* 2005) and evidence of late Quaternary deformation in the Palmyrides (e.g. Abou Romieh *et al.* 2009).

Fig. 4 depicts the GPS velocities resolved along a NNW–SSE profile across central Syria (see Fig. 2 for location), and roughly perpendicular to the strike of the Palmyride fold belt. In general, the sites shown in these profiles are located sufficiently far from the major faults so that they likely are not affected by transient, elastic strains. The velocities in the NNW–SSE direction (Fig. 4a) demonstrate ~1 mm yr^{-1} of consistent motion between the southern two sites relative to the rest of the profile points in northern Syria. These two sites are located within and south of the Palmyride fold belt, and their motion is also consistent with the southernmost site in Syria. Although the uncertainties are relatively large and the station spacing is sparse, the motion of the southern vectors (also including the southernmost site in Syria, shown in Fig. 2) is coherent and distinct from the overall motion of the sites at the northern end of the profile. Additionally, this is consistent with one reverse-fault focal
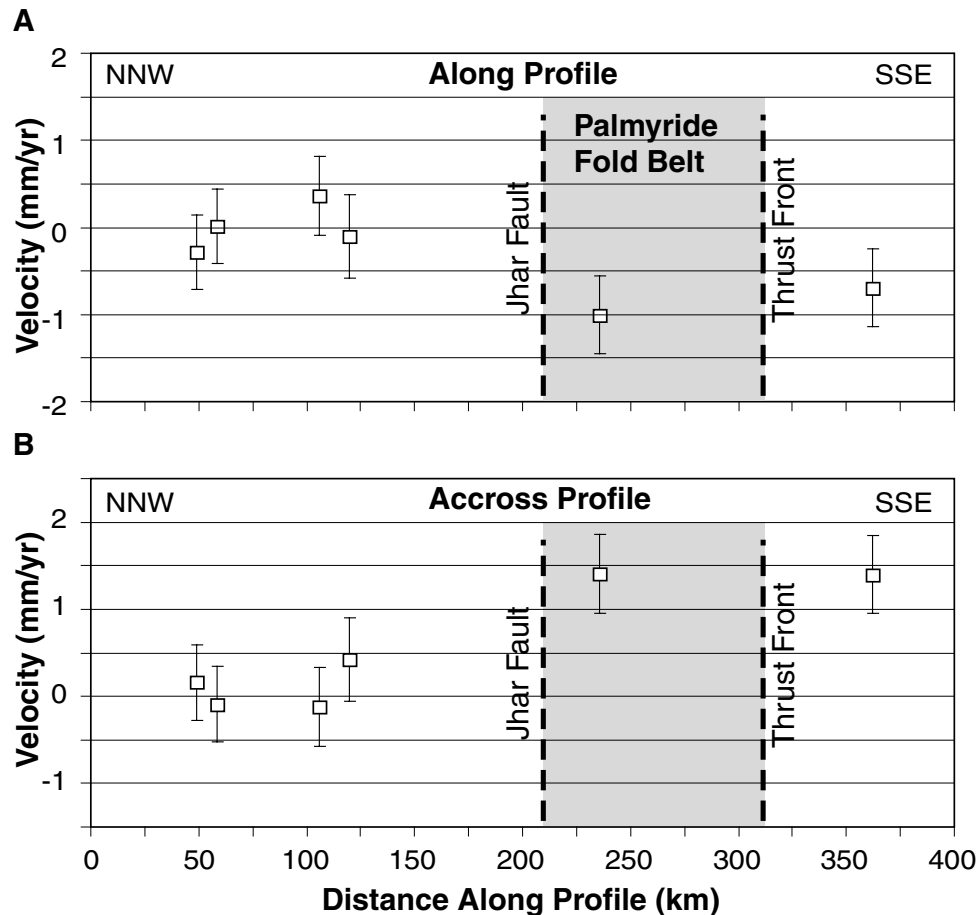

Figure 4. Plots showing GPS velocities (a) parallel and (b) perpendicular to the NNW–SSE profile across northwestern Arabia (oriented perpendicular to the main strike of the Palmyride fold belt; see Fig. 2 for profile location). A systematic offset between sites north and south of the Palmyride fold belt suggests up to 1 mm yr^{-1} of contraction and possible left-lateral shear along the Jhar fault.

mechanism shown in Fig. 1. Hence, we suggest the GPS data may reflect up to 1 mm yr^{-1} of active, regional shortening, although the level of uncertainty in these data precludes assessing the kinematics of specific structures within the Palmyride fold belt.

In the ENE–WSW direction (parallel to the strike of the Jhar fault and the structural trend of the Palmyride fold belt), the southern GPS sites also demonstrate consistent ENE motion relative to the sites located north of the Palmyride fold belt (Fig. 4b). Although the differential motion falls generally within the uncertainties of the velocities, we suggest that these velocities might be the results of up to 0.5–1.0 mm yr^{-1} of left-lateral slip along the Jhar fault. Such lateral shear is consistent with the earthquake focal mechanisms reported for recent earthquakes in the Palmyrides (e.g. Chaimov *et al.* 1990; Salamon *et al.* 2003; Fig. 1).

5 DISCUSSION

The GPS results demonstrate that the northern DSFS is actively shearing and accumulating strain, contrasting with previous suggestions, based in part on a paucity of seismicity, that the northern DSFS has become inactive (e.g. Girdler 1990; Butler *et al.* 1997, 1998). Furthermore, the present-day slip rates may reflect the longer-term (late Cenozoic) tectonism of the northern Dead Sea fault. The geodetic-derived slip rate reported here is similar to the long-term estimate of 3.3–4.0 mm yr^{-1} reported by Gomez *et al.* (2006) based on an apparent displacement of a large, Pliocene volcano in NW Syria. More significantly, the present-day contraction across the Palmyride fold belt and the slower slip rate along the northern DSFS appear to reflect the long-term deficit in total geological slip between the northern and southern DSFS (Chaimov *et al.* 1990). Hence, this regional partitioning of deformation has likely persisted through the Late Cenozoic.

Our geodetic slip rate is lower than (and statistically distinct from) predictions from well-constrained, plate tectonic models (e.g. Wdowinski *et al.* 2004; Reilinger *et al.* 2006)—hence, there appears to be a northward decrease, rather than the predicted increase, in the slip rate of the DSFS. Additionally, this northward decrease cannot be completely explained by shortening within northern Arabia (i.e. the Palmyride fold belt)—there is a distinct velocity gradient within the Sinai Plate between NW Syria and northern Lebanon. Furthermore, the predicted convergence across the northern DSFS is not apparent in the GPS velocities; within the uncertainties, the GPS data suggest neither contraction nor extension across the DSFS.

In summary, the GPS velocities demonstrate that the kinematics of the northern DSFS deviate significantly from plate tectonic predictions based on models that consider the Arabian and Sinai plates to be rigid. Both the Sinai and Arabian plates actively converge with Eurasia. However, whereas N–S GPS velocities on the Arabian Plate decrease northward across the Palmyride fold belt, N–S GPS velocities on the Sinai Plate increase at the latitude of northern Lebanon. In an Arabia-fixed reference frame, this is expressed as the northward decrease in velocity of sites on the Sinai Plate that is observed in northern Lebanon and NW Syria (Fig. 2)—that is, a spatially abrupt and statistically significant velocity gradient exists between the relatively coherent GPS velocities in central & southern Lebanon versus those in northern Lebanon and NW Syria (see profiles in Fig. 2). The nature of this velocity gradient requires N–S extension.

As one possible hypothesis, we suggest that the NE part of the Sinai Plate may be broken and partially decoupled from the southern part of the 'plate' (Fig. 5). In this case, the northern DSFS would reflect relative motion between Arabia and this smaller block, rather
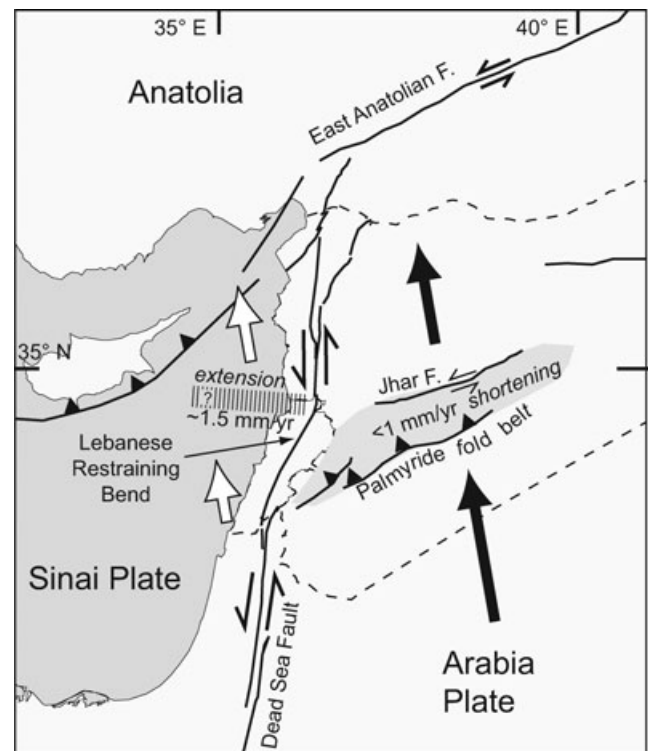
Figure 5. Conceptual model illustrating the motion of the northwestern Arabia Plate (large black arrow) and the northeastern Sinai Plate (large white arrow) relative to Eurasia. Total predicted plate motion of northwestern Arabia is decomposed into transpression across the Palmyride fold belt (PFB) and north–south strike-slip along the DSFS, resulting in a northward decrease in motion of Arabia relative to Eurasia. Based on the velocity gradient shown by the GPS data, we suggest ∼N–S extension within the small, Sinai Plate, near the northern end of the Lebanese Restraining Bend to account for (1) the observed northward decrease in GPS velocities within the Sinai Plate and (2) the decrease in slip rate on the N segment of the DSFS. Although the GPS demonstrate N–S extension near the DSFS, the western limit of the extension is not constrained; hence it is denoted with a question mark. *Note:* Length of arrow schematically depicts the magnitude of motion, but arrows are not drawn to scale.

than the larger Sinai Plate. Such a hypothesis explains the observed extensional velocity gradient in northern Lebanon. Late Cenozoic, horizontal extension in this area would also be consistent with the Neogene and Quaternary alkali volcanic activity observed at the northern part of the restraining bend (Mouty *et al.* 1992). Alternatively, N–S extension may be localized to the vicinity of the DSFS. Furthermore, a single structure bounding such a block (and linking it to the Sinai–Anatolia plate boundary) is not clearly expressed in the topography, nor evident on existing geological maps, suggesting that this horizontal extension, if occurring over geological timescales, would be spatially distributed. Further geophysical and geological observations are needed to test this preliminary hypothesis.

In terms of the earthquake hazard, the lower slip rate also suggests that the 800-yr seismic quiescence along the Misyaf fault (Meghraoui *et al.* 2003) may not necessarily represent a seismic gap. Assuming an average coseismic slip of 4.5 m (one-third of the offset of the faulted Roman aqueduct reported by Meghraoui *et al.*), the 2.5 mm yr^{-1} slip rate would be consistent with an average recurrence period of 1800 yr. However, owing to the clearly non-periodic behaviour of the northern DSFS (Meghraoui *et al.* 2003), the appropriateness of such a calculation is questionable. In addition, the GPS velocities indicate present-day tectonism in the Palmyride fold belt,

which should also be considered within the context of the regional earthquake hazard.

6 CONCLUSIONS

The GPS results presented herein provide direct geodetic measurement of present-day fault slip along the northern DSFS in Syria and within the northwestern part of the Arabian Plate. The deformation is reasonably well constrained by GPS measurements spanning 7.5 yr yielding velocities with 1σ uncertainties generally less than 0.6 mm yr^{-1}.

The GPS velocities in Syria demonstrate along-strike variations from the central and southern DSFS, which suggest that the DSFS may not behave as a 'simple' transform. Although inferring fault slip rates from geodetic data is inherently model dependent, the 1-D dislocation models shown here demonstrate that the northern DSFS is kinematically distinct from the central and southern parts of the transform—namely, the slip rate appears to be significantly slower than the central and southern sections of the transform. Shortening across the Palmyride fold belt may account for some of this slip deficiency, but there is also a distinct GPS velocity gradient within the Sinai Plate itself. We speculate that active, N–S extension of the Sinai micro plate near the northern end of the DSFS in Lebanon may account for the reduced slip on the northern fault segment in Syria. Hence, the tectonic configuration of the northeastern Mediterranean region is likely more complicated than previously thought.

ACKNOWLEDGMENTS

REFERENCES

Abou Romeih, M. *et al*., 2009. Active crustal shortening in NE Syria revealed by deformed terraces of the River Euphrates, *Terra Nova,* in press.

Akyuz, H.S., Altunel, E., Karabacak, V. & Yalciner, C.C., 2006. Historical earthquake activity of the northern part of the Dead Sea Fault Zone, southern Turkey, *Tectonophysics,* **426,** 281–293.

Allen, M., Jackson, J. & Walker, R., 2004. Late Cenozoic reorganization of the Arabia-Eurasia collision and the comparison of short-term and long-term deformation rates, tectonics, *Tectonics,* **23,** TC2008, doi:2010.1029/2003TC001530.

Ambraseys, N.N. & Barazangi, M., 1989. The 1759 earthquake in the Bekaa Valley: implications for earthquake hazard assessment in the Eastern Mediterranean region, *J. geophys. Res.,* **94,** 4007–4013.

Ambraseys, N.N. & Jackson, J.A., 1998. Faulting associatd with historical and recent earthquakes in the Eastern Mediterranean region, *Geophys. J. Int.,* **133,** 390–406.

Brew, G., Litak, R., Barazangi, M. & Sawaf, T., 1999. Tectonic evolution of Northeast Syria: regional implications and hydrocarbon prospects, *GeoArabia,* **4,** 289–318.

Brew, G., Lupa, J., Barazangi, M., Sawaf, T., Al-Imam, A. & Zaza, T., 2001. Structure and tectonic development of the Ghab basin and the Dead Sea fault system, Syria, *J. geol. Soc. Lond.,* **158,** 665–674.

Butler, R.W.H., Spencer, S. & Griffiths, H.M., 1997. Transcurrent fault activity on the Dead Sea Transform in Lebanon and its implications for plate tectonics and seismic hazard, *J. geol. Soc. Lond.,* **154,** 757–760.

Butler, R.W.H., Spencer, S. & Griffiths, H.M., 1998. The structural response to evolving plate kinematics during transpression: evolution of the Lebanese restraining bend of the Dead Sea Transform, in *Continental Transpressional and Transtensional Tectonics,* pp. 81–106, eds. Holdsworth, R.E., Strahan, R.A. & Dewey, J.F., Geological Soc. London, London.

Chaimov, T.A., Barazangi, M., Al-Saad, D., Sawaf, T. & Gebran, A., 1990. Crustal shortening in the Palmyride fold belt, Syria, and implications for movement along the Dead Sea fault system, *Tectonics,* **9,** 1369–1386.

Daeron, M., Klinger, Y., Tapponnier, P., Elias, A., Jacques, E. & Sursock, A., 2007. 12,000-year long Record of 10 to 13 Paleo-Earthquakes on the Yammouneh Fault (Levant Fault System, Lebanon), *Bull. seism. Soc. Am.,* **97,** 749–771.

Dong, D., Herring, T.A. & King, R.W., 1998. Estimating regional deformation from a combination of space and terrestrial geodetic data, *J. Geod.,* **71,** 200–211.

Ferry, M., Meghraoui, M., Karaki, N.A., Al-Taj, M., Amoush, H., Al-Dhaisat, S. & Barjous, M., 2007. A 48-kyr-long slip rate history for the Jordan Valley segment of the Dead Sea Fault, *Earth planet. Sci. Lett.,* **260,** 394–406.

Freund, R., Garfunkel, Z., Zak, I., Goldberg, M., Weissbrod, T. & Derin, B., 1970. The shear along the Dead Sea rift, *Phil. Trans. R. Soc. Lond.,* **267,** 107–130.

Girdler, R.W., 1990. The Dead Sea transform fault system, *Tectonophysics,* **180,** 1–13.

Gomez, F. *et al*., 2007. Global Positioning System measurements of strain accumulation and slip transfer through the restraining bend along the Dead Sea fault system in Lebanon, *Geophys. J. Int.,* **168,** 1021–1028.

Gomez, F., Khawlie, M., Tabet, C., Darkal, A.N., Khair, K. & Barazangi, M., 2006. Late Cenozoic uplift along the northern Dead Sea transform in Lebanon and Syria, *Earth planet. Sci. Lett.,* **241,** 913–931.

Gomez, F. *et al*., 2003. Holocene faulting and earthquake recurrence along the Serghaya branch of the Dead Sea fault system in Syria and Lebanon, *Geophys. J. Int.,* **153,** 658–674.

Hatcher, R.D., Jr., Zietz, I., Regan, R.D. & Abu-Ajamieh, M., 1981. Sinistral strike-slip motion on the Dead Sea Rift; confirmation from new magnetic data, *Geology,* **9,** 458–462.

Hempton, M.R., 1987. Constraints on Arabian plate motion and extensional history of the Red Sea, *Tectonics,* **6,** 687–705.

Herring, T.A., King, R.W. & McClusky, S.C., 1997. Geodetic constraints on interseismic, coseismic, and postseismic deformation in southern California, Annual Report to SCEC.

Joffe, S. & Garfunkel, Z., 1987. Plate kinematics of the circum Red Sea–a re-evaluation, *Tectonophysics,* **141,** 5–22.

King, R.W. & Bock, Y., 1998. Documentation of MIT GPS Analysis Software: GAMIT, Massachusetts Institute of Technology, Cambridge, MA.

Klinger, Y., Avouac, J.P., Abou Karaki, N., Dorbath, L., Bourles, L. & Reys, J., 2000. Slip rate on the Dead Sea transform fault in the northern Araba Valley (Jordan), *Geophys. J. Int.,* **142,** 755–768.

Le Beon, M. *et al*., 2008. Slip rate and locking depth from GPS profiles across the southern Dead Sea Transform, *J. geophys. Res.,* **113,** B11403, doi:11410.11029/12007JB005280.

Lisowski, M., Savage, J.C. & Prescott, W.H., 1991. The velocity field along the San Andreas fault in central and southern California, *J. geophys. Res.,* **96,** 8369–8389.

Litak, R.K., Barazangi, M., Beauchamp, W., Seber, D., Brew, G., Sawaf, T. & Al-Youssef, W., 1997. Mesozoic-Cenozoic evolution of the intraplate Euphrates fault system, Syria: implication for regional tectonics, *J. geol. Soc. Lond.,* **154,** 653–666.

Mahmoud, S., Reilinger, R., McClusky, S., Vernant, P. & Tealeb, A., 2005. GPS evidence for northward motion of the Sinai block: implications for E. Mediterranean tectonics, *Earth planet. Sci. Lett.,* **238,** 217–227.

Mao, A., Harrison, C. & Dixon, T., 1999. Noise in GPS coordinate time series, *J. geophys. Res.,* **104,** 2797–2816.

Marco, S., Stein, M. & Agnon, A., 1996. Long-term earthquake clustering: a 50,000-year paleoseismic record in the Dead Sea Graben, *Geophys. J. Int.,* **101,** 6179–6191.

McClusky, S. *et al.*, 2000. Global Positioning System constraints on plate kinematics and dynamics in the eastern Mediterranean and Caucasus, *J. geophys. Res.,* **105,** 5695–5719.

Meghraoui, M. *et al.*, 2003. Evidence for 830 years of seismic quiescence from palaeoseismology, archaeosesimology, and historical seismicity along the Dead Sea fault in Syria, *Earth planet. Sci. Lett.,* **210,** 35–52.

Mouty, M., Delaloye, M., Fontignie, D., Piskin, O. & Wagner, J.-J., 1992. The volcanic activity in Syria and Lebanon between Jurassic and Actual, *Schweiz. Mineral. Petrogr. Mitt.,* **72,** 91–105.

Nemer, T., Gomez, F., Haddad, S. & Tabet, C., 2008. Coseismic growth of sedimentary basins along the Yammouneh strike-slip fault (Lebanon), *Geophys. J. Int.,* **175,** 1023–1039.

Pearson, C., Denys, P. & Hodgkinson, K., 2000. Geodetic constraints on the kinematics of the Alpine Fault in the southern South Island of New Zealand, using results from the Hawea-Haast GPS transect, *Geophys. Res. Lett.,* **27,** 1319–1322.

Quennell, A.M., 1984. The Western Arabia rift system, in *The Geological Evolution of the Eastern Mediterranean,* pp. 775–788, eds Dixon, J.E. & Robertson, A.H.F., Blackwell Scientific, Oxford.

Reilinger, R. *et al.*, 2006. GPS Constraints on Continental deformation in the Africa-Arabia-Eurasia continental collision zone and implications for the dynamics of plate interactions, *J. geophys. Res.,* **111,** doi:10.1029/2005JB004051.

Salamon, A., Hofstetter, A., Garfunkel, Z. & Ron, H., 1996. Seismicity of the eastern Mediterranean region: Perspective from the Sinai subplate, *Tectonophysics,* **263,** 293–305.

Salamon, A., Hofstetter, A., Garfunkel, Z. & Ron, H., 2003. Seismotectonics of the Sanai subplate–the eastern Mediterranean region, *Geophys. J. Int.,* **155,** 149–173.

Sandvol, E. & Hearn, T., 1994. Bootstrapping shear-wave splitting errors, *Bull. seism. Soc. Am.,* **84,** 1971–1977.

Savage, J.C. & Burford, R.O., 1973. Geodetic determination of relative plate motion in central California, *J. geophys. Res.,* **78,** 832–845.

Sbeinati, M.R., Darawcheh, R. & Mouty, M., 2005. Catalog of historical earthquakes in and around Syria, *Ann. Geofis.,* **48,** 347–435.

Segall, P., 2002. Integrating geologic and geodetic estimates of slip rate on the San Andreas fault system, *Int. Geol. Rev.,* **44,** 62–82.

Wdowinski, S. *et al.*, 2004. GPS measurements of current crustal movements along the Dead Sea Fault, *J. geophys. Res.,* **109,** doi:10.1029/2003JB002640.

Westaway, R., 2004. Kinematic consistency between the Dead Sea Fault Zone and the Neogene and Quaternary left-lateral faulting in SE Turkey, *Tectonophysics,* **391,** 203–237.

Wright, T., Parsons, B. & Fielding, E., 2001. Measurement of interseismic strain accumulation across the North Anatolian Fault by satellite radar interferometry, *Geophys. Res. Lett.,* **28,** 2117–2120.

Zhang, J., Bock, Y., Johnson, H., Fang, P., Williams, S., Genrich, J., Wdowinski, S. & Behr, J., 1997. Southern California Permanent GPS Geodetic Array: error analysis of daily position estimates and site velocities, *J. geophys. Res.,* **102,** 18 035–18 055.